DIRECT NUMERICAL SIMULATIONS OF TURBULENCE OVER TWO-DIMENSIONAL PERMEABLE RIBS

WORKSHOP
Direct and Large-Eddy Simulation 13
October 26th-29th 2022, Udine, Italy

DIRECT NUMERICAL SIMULATIONS OF TURBULENCE OVER TWO-DIMENSIONAL PERMEABLE RIBS

Y. Kuwata[1] **and K.Suga**[1]
[1] Department of Mechanical Engineering
Osaka Metropolitan University, Japan
kuwata@omu.ac.jp

INTRODUCTION

Turbulent flows over a rough surface are ubiquitous in engineering applications, and numerous studies have been undertaken to reveal the effects of roughness on turbulent flows. However, the roughness elements discussed so far have been impermeable despite the fact that roughness usually have a permeability. Examples include the river bed and vegetation canopy. This serves as a motivation to discuss the effects of permeable roughness.

Recently, the effects of the permeable roughness was experimentally studied by the author's group [1]. They showed that the roughness-induced drag force was decreased with increasing the permeability. The discussions on the log-law parameters including the zero-plane displacement and equivalent roughness suggested that the permeability increased the zero-plane displacement but decreased the equivalent roughness. However, owing to limited optical access, the flow physics around the permeable roughness remains not completely clear. The purpose of the present study is to shed light on the underlying physics on the effects of the permeable roughness by using the high-fidelity direct numerical simulation data.

METHODOLOGY

A schematic of a rough-walled channel flow is shown in Figure1. The top and bottoms walls were impermeable smooth walls, whereas the porous wall with two-dimensional transverse porous-ribs were considered in the bottom of the channel. The rib height was $k = 0.1H$ with H being the distance from the rib bottom to the top wall, and the separation between the neighboring ribs was varied: $w = k$ and $9k$. The flow was periodic in the streamwise (x) and spanwise (z) directions. The flow was driven by a streamwise pressure difference which was adjusted so as to yield the desired flow rate for the bulk mean Reynolds number of $Re_b \simeq 5500$. The size of the computational domain was $5H$ and $1.5H$ in the streamwise and spanwise directions, respectively. The porous medium under consideration consisted of the Kelvin cells (or tetrakaidecahedrons). The porosity of the porous medium was fixed at $\varphi = 0.8$, while we considered two permeability cases: one was the high permeable "HP" case, and the other was low permeable "LP" case. The size of a single Kelvin-cell unit for cases HP and LP were $D = 0.1H$ and $D = 0.05H$, respectively, and the resulting permeabilities were $K/k^2 = 6.4 \times 10^{-5}$ and 1.7×10^{-5}, respectively. The thicknesses of the porous wall were $h = 3D$ for case HP and $h = 2D$ for case LP. The transverse rib was comprised of $1(x) \times 1(y) \times 15(z)$ cells for case HP and $2(x) \times 2(y) \times 30(z)$ cells for case LP. The geometry of the porous-rib roughness was shown in Figure2.

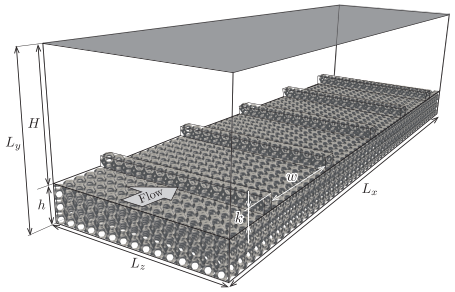

Figure 1: Flow geometry of a porous-rib channel flow.

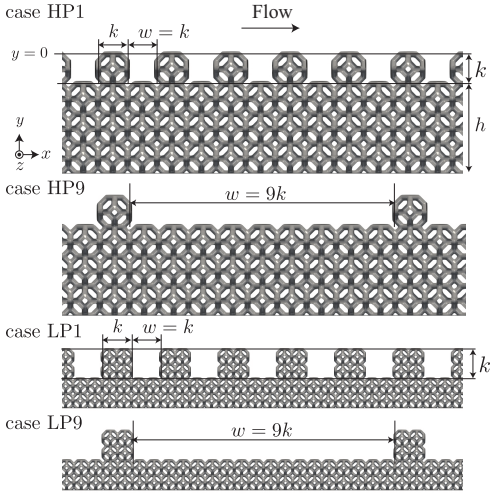

Figure 2: Geometry of the porous-rib roughness: the name of case consists of two letters follower by a number. The letters take "HP" or "LP", and the number stands for the value of w/k.

For the present DNSs, we used the three-dimensional 27 discrete velocities multiple relaxation time LBM [2]. This LBM model was originally developed by the author's group and has successfully been applied to turbulent flows over resolved porous and rough walls [3]. A single Kelvin-cell unit

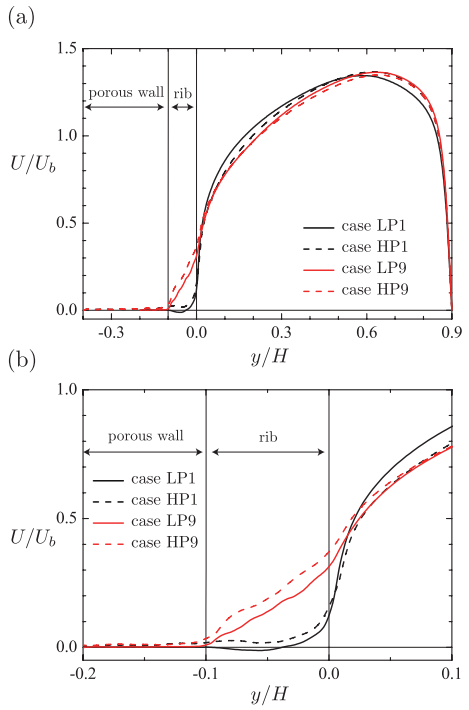

Figure 3: (a) streamwise mean velocity normalized by the bulk mean velocity U_b, (b) enlarged figure near the porous-rib.

was resolved by $40(x) \times 40(y) \times 40(z)$ grids, yielding to the grid spacings in wall units for cases HP and LP are $\Delta^+ \simeq 1.8$ and 0.7, respectively. The total number of grids were 0.4 and 1.30 billions, respectively.

RESULTS AND DISCUSSIONS

Figure 3 presents profiles of $x-z$ plane-averaged streamwise mean velocity U. In Fig.3(a), all the profiles are significantly skewed, that is, the maximum mean velocity location shifts toward the top wall, which is due to an increased frictional resistance by the porous-ribs. The inspection of the mean velocity near the porous-rib in Fig. 3(b) shows that a reduction in U by the porous-rib is larger for $w/k = 1$ as expected. For case LP1, we observe a negative mean flow in the porous-rib region ($-0.1 < y/H < 0$), whereas the negative flow region is washed out by the increased permeability (case HP1).

To better understand the effects of the permeability on the frictional resistance, Figure 4 compares the drag coefficient C_D, which is defined based on the total shear stress at the rib bottom ($y = -k$) [1]. The reference experimental data are for two-dimensional transverse metallic foam ribs [1] where the permeability for case #30 is 70% lower than that for case LP, and that for case #13 is 30% lower than that for case HP. The figure confirms that for the present DNS data, an increase in the rib separation w/k results in an increase in C_D, and the dependence of w/k is more significant for case LP. This suggests that the effects of the rib arrangement is weakened by the permeability, and this trend is qualitatively similar to the experimental data.

Finally, to obtain physical understanding on the effects of the permeability on C_D, we analyze the FIK identity [4] which decomposes the friction factor into the physically understandable contributors. Following [4], we derived the contributors

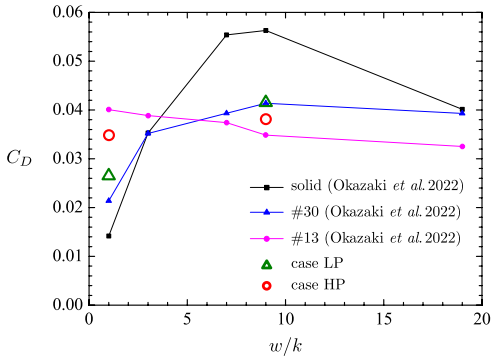

Figure 4: Comparison of the drag coefficient C_D with the experimental data [1].

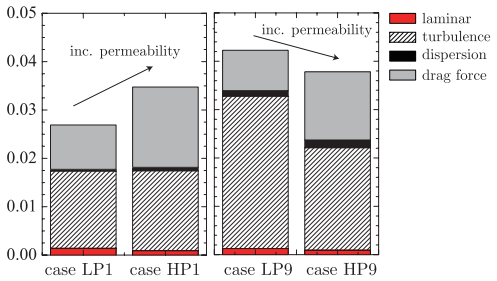

Figure 5: Contribution to the drag coefficient C_D.

to C_D based on the $x-z$ plane- and time-averaged momentum equation. For the present flows, the dispersion and drag-force contributions appear as well as the laminar and turbulence contributions. The dispersion contribution accounts for the dispersive covariance, which is generated by the streamwise and spanwise inhomogeneity of the mean velocity [3]. The drag force contribution accounts for the viscous and pressure drags offered by the porous-ribs. Those contributions are shown in Figure5. The first notable observation is that the turbulence and drag force contributions dominate C_D, whereas the laminar and dispersion contributions are negligibly small. For cases with $w/k = 1$, the drag force contribution is increased by the permeability, while the turbulence contribution is almost unchanged. The increased drag force contribution is considered to be due to the increased penetrating flow through the porous rib. The drag force contribution also increases with the permeability for cases with $w/k = 9$; however, the rib-induced turbulence generation is attenuated by the increased permeability, leading to a decrease in the turbulence contribution with the permeability. As a result, the C_D value for cases with $w/k = 9$ decreases with increasing the permeability.

REFERENCES

[1]Okazaki, Y. *et al.* : Turbulent channel flows over porous rib-roughed walls. *Exp. Fluids*, **63.4**, 1-20(2022).

[2]Suga, K. et al. *et al.* : A D3Q27 multiple-relaxation-time lattice Boltzmann method for turbulent flows. *Compt. Math. Appl.*, **69.6**, 518-529 (2015).

[3]Kuwata, Y., & Suga, K. : Lattice Boltzmann direct numerical simulation of interface turbulence over porous and rough walls. *Int. J. Heat Fluid Flow*, **61**, 145-157 (2016).

[4]Fukagata, K., Iwamoto, K., & Kasagi, N. : Contribution of Reynolds stress distribution to the skin friction in wall-bounded flows. *Phys. Fluids*, **14(11)**, L73-L76 (2002).